Dynamics of femtosecond laser produced tungsten nanoparticle plumes

S. S. Harilal,[1] N. Farid,[1,2] A. Hassanein,[1] and V. M. Kozhevin[3]
[1]*Center for Materials Under Extreme Environment, School of Nuclear Engineering, Purdue University, West Lafayette, Indiana 47907, USA*
[2]*School of Physics and Optical Engineering, Dalian University of Technology, Dalian 116024, China*
[3]*Ioffe Physics Technical Institute, Russian Academy of Sciences, St. Petersburg 194021, Russia*

(Received 23 September 2013; accepted 11 November 2013; published online 22 November 2013)

We investigated the expansion features of femtosecond laser generated tungsten nanoparticle plumes in vacuum. Fast gated images showed distinct two components expansion features, viz., plasma and nanoparticle plumes, separated by time of appearance. The persistence of plasma and nanoparticle plumes are ~500 ns and ~100 μs, respectively, and propagating with velocities differed by 25 times. The estimated temperature of the nanoparticles showed a decreasing trend with increasing time and space. Compared to low-Z materials (e.g., Si), ultrafast laser ablation of high-Z materials like W provides significantly higher nanoparticle yield. A comparison between the nanoparticle plumes generated by W and Si is also discussed along with other metals. [http://dx.doi.org/10.1063/1.4833564]

I. INTRODUCTION

Nanoparticle production and application research is an area of significant scientific interest essentially due to wide variety of potential applications especially in the emerging sectors such as bio and medical technology.[1] Nanoparticles, which act as a bridge between the atomic and molecular structures and bulk materials, have numerous future energy applications ranging from nano-photovoltaic to nano-photonics.[2,3] Metal nanoparticles with unique plasmonic properties have extensive applications in the fields of medicine and photonics.[4,5] However, it has to be pointed out that the performance of nanomaterials for various applications depends on their distribution, size, and shape and hence precise control over their growth is essential. The fine control over the formation of nanomaterial synthesis and repeatability will lead to cost effectiveness as well as large scale manufacturing which are prerequisite from the technological standpoint. Moreover, the nanoparticle production yield should be higher for a cost effective way for various applications. Typical synthesis methods for nanoparticles are liquid, gas, and vapor phases.

Laser ablation plumes are well known as a source of nanoparticle generation and intense research is underway in the last few years especially for identifying physical mechanisms leading to nanoparticle production though it is still unclear.[6–16] In order to understand the processes leading to nanoparticle formation, the mechanism of plasma plume generation from the target material under laser irradiation and the interaction of the resulting plume with the ambient atmosphere in the plasma chamber should be studied in detail.[17,18] The properties of laser ablation depends on numerous laser, target and environmental parameters and hence there is a possibility of precise control over nanoparticles size as well as their size distribution. However, this is possible only through fundamental understanding of nanoparticle formation especially how, when, and where these particles are formed in ablation plumes. Even though all natural and laboratory plasmas are a source of nanoparticles, recent research showed that nano-meter size range nanoparticles can be produced efficiently with the use of ultrafast laser ablation.[6,15,19,20] However, extensive research efforts are necessary to develop clear understanding of physical mechanisms leading to nanoparticle formation during ultrafast laser ablation.[21] Previous studies showed that ultrafast laser ablation leads to generation of nanoparticles which was temporally separated from the atomic plume.[9,22–24] Recent results showed that nanoparticle generation during laser ablation in the presence of a liquid is an efficient and unique technique to produce large variety of nanoclusters in a scalable manner with certain properties.[8,14] However, similar to nanoparticle generation during laser ablation in vacuum, the exact nanoparticle formation mechanism during and after cavitation in liquid confinement is still not fully understood.

In this article, we investigated nanoparticle formation in tungsten plasma generated using femtosecond laser. A multitude of plume diagnostic tools were used for analyzing plasma and nanoparticles. Our results highlight significantly higher nanoparticle yield during ultrafast laser ablation of high-Z material like W compared to low-Z material like Si.

II. EXPERIMENTAL DETAILS

The fs laser used for generating W plasma consists of a mode-locked Ti-sapphire oscillator, stretcher, regenerative amplifier, multi-pass amplifier and a compressor giving 10 Hz, 800 nm, 40 fs pulses with an energy ~6 mJ. The energy of the fs laser beam was controlled using a half-waveplate and polarizer positioned before the compressor optics.[25] The laser beam was focused on targets of interest at normal incidence with a spot size of ~300 μm and with a laser fluence of ~8 J/cm^2 (power density ~2×10^{14} W/cm^2). The target was posited on an x-y translator for providing fresh surface and all experiments were performed in vacuum with a base pressure ~10^{-6} Torr. We used fast gated imaging employing intensified CCD (ICCD), optical emission spectroscopy (OES), and time of flight (TOF) emission spectroscopy for analyzing plasma plume.[25] The ICCD camera was

synchronized with arrival of laser beam using a timing generator. The plume emission images at the earliest times (<100 ns) were obtained with 2 ns gate width and at later times a 5% width of the gate delay was used for compensating reduction in plasma intensity. A 0.5 m triple grating spectrograph with an ICCD detector was used for recording the emission features of the plasma while the TOF emission features were captured using 2 ns rise time photomultiplier tube (PMT) which was attached to one of the two exit ports of the spectrograph. The particle size distribution analysis has been carried out using witness plates in conjunction with atomic force microscope (AFM).

III. RESULTS AND DISCUSSION

The laser-target interaction leads to the formation of a bright plasma that emits profoundly in the visible region. Among the various plasma diagnostic tools, fast photography in the visible region is one of the simplest and it provides two-dimensional snap shots of the three-dimensional plume propagation with detailed information about expansion dynamics. Typical ICCD images of the expanding W plume at different times after the onset of plasma formation are given in Figure 1. In fs LA, an ablation plume is generated at significantly later times compared to laser pulse duration.[26] This is due to shorter duration of the laser pulse compared to characteristic relaxation times, such as the electron-to-ion energy transfer time, electron heat conduction time, and hence the hydrodynamic or expansion time; all of which typically occur on the order of several picoseconds after the laser absorption by the target. The images given in Figure 1 showed distinct emission features in the visible region with increasing time of evolution. The duration of the intensification (exposure time) was set at 2 ns for collecting images at early times (<100 ns), while a 5% gate width with respect to the gate delay was used for capturing plume self-emission at later times for compensating the reduction in intensity and each image is obtained from a single laser pulse. Timing jitter was less than 1 ns. All images shown here have been normalized by the peak intensity in that image for better viewpoint.

Regardless of the pulse width of the exciting laser, plasma expansion into a vacuum environment is simply adiabatic and can be fully predicted by theoretical models and numerical gas dynamic simulations.[27,28] The plume propagation in vacuum is governed by the initial pressure gradients in the plume at the early times during its creation and the spot size. Typically, fs LA plumes are found to be more cylindrical compared to long-pulse ns LA due to rapid deposition of laser energy density and hence higher pressure gradient.[25,29] The plume images given in Figure 1 clearly showed two components and their expansion features are separated in time. A fast component appears at early time moves with a high expansion velocity and finally disappears after ~400 ns (left column in Figure 1). However, the ablation spot at the target is found to be more brighter with increasing time and expand considerably slower compared to the fast component noticed at early times which gives rise to second plume component (right column in Figure 1). The second component also persisted for an elongated time. The

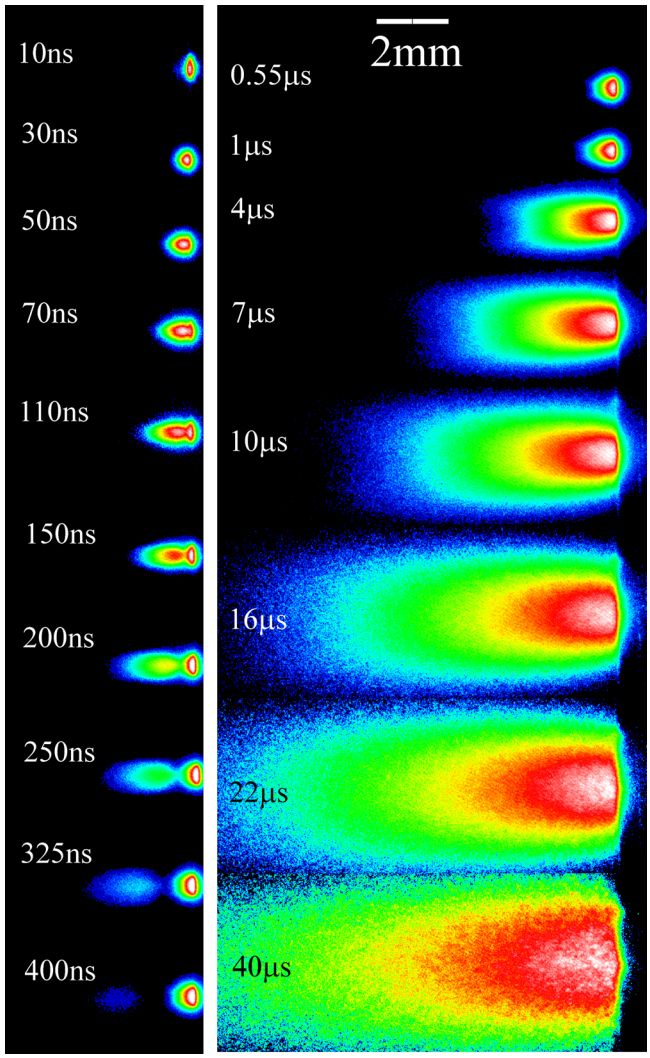

FIG. 1. ICCD images of W plasma and nanoparticles plumes generated using 40 fs, 800 nm ultrafast laser in vacuum. The laser beam was focused on the target at normal incidence and the spectrally integrated light emission was collected orthogonally using a fast gated camera. The ICCD gating was set at 5% of gate width and each image was normalized to its maximum intensity for better view.

multicomponent structure of femtosecond laser ablation plumes separated in time have been observed previously by several groups.[9,22–24]

The emission intensity as a function of distance along the direction of plume expansion and position of the plume front at different times during its evolution are shown in Figures 2(a) and 2(b). The spatial dependence of emission intensity is obtained from the ICCD images along the target normal by averaging 3 pixel intensities orthogonal to plume expansion axis and it provides useful information about the internal structures in the plume. There are several interesting features of these plots worth noting. At earliest times (<70 ns), the emission intensity profiles showed single peak distribution after the onset of plasma formation. However, with time, the plasma detached from the core region showing plume splitting (Figure 2(a)). The detached plasma emits weakly at later times and almost disappears at times >400 ns. The intense peak noticed at shorter distances evolves slowly and its evolution history is given in Figure 2(b) at later times.

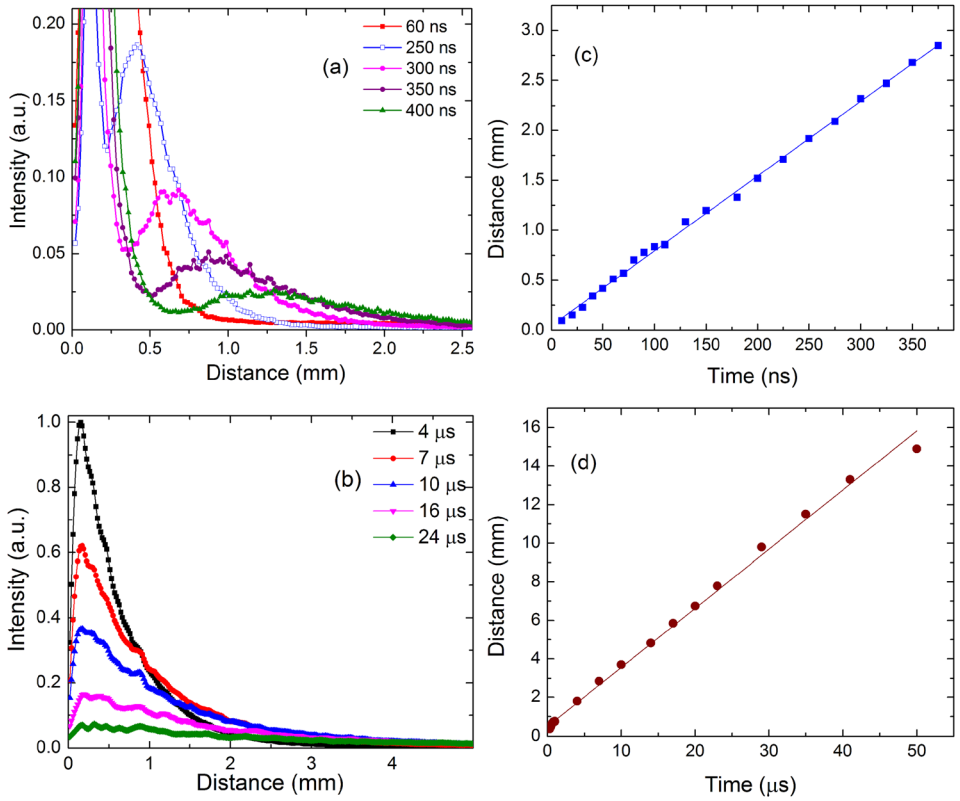

FIG. 2. Emission intensity counts obtained from the ICCD images along the plume expansion direction are given for various times after evolution of the plasma. The emission intensity counts at earlier times are highlighted in (a) and in (b) the intensity counts for slower component are given. (c) and (d) show the approximate plume front position for faster and slower components, respectively. The plume front position is obtained by considering the respective position corresponds to 10% of the maximum intensity. In (a), the intensity of the faster peak (plasma plume) is showed as saturated for highlighting the evolution of nanoparticle plume.

Unlike the fast component, where the peak of the emission moves to farther distances with time, the intensity peak of the slower component is found to be maximum near the target surface. The second plume component moves with much slower velocity and its intensity drops with increasing distance from the target. The position–time (R-t) plot obtained from the images is shown in Figures 2(c) and 2(d) for both fast and slow components of the plume. Since all measurements were performed in vacuum, shock wave generation at the plume boundary is absent which is seen routinely in the presence of moderate to higher ambient gas pressures.[30] Hence for obtaining plume front positions 10% of the maximum intensity is considered and these plots approximately provide expansion velocities for the faster and slower plumes. Both plume components followed free expansion in vacuum indicated by linear line fits. The estimated velocities are 8×10^5 cm/s and 3×10^4 cm/s for faster and slower components, respectively. The two components plume structure with varying expansion dynamics have been observed previously for Si, Cu, and Au targets.[6]

The spectral features obtained from the fast and slow components are given in Figure 3. We utilized OES for examining emission features of plasma at various times after the onset of plasma formation. Both the spectra were recorded at a distance 1 mm from the target and at different times (a) 200 ns and (b) 2 μs. At early times and close to the target, intense continuum emission dominates along with line emission. The continuum radiation, or bremsstrahlung, occurs when a free electron collides with another particle and makes a transition to another free state of lower energy, with the emission of photons. The line emission features from the faster component are predominantly dominated by excited W neutrals. Previous reports showed that the fs laser ablation plumes profoundly emit atomic species compared to ns laser excitation where laser-plasma heating ionization is prevalent at early times.[29,31] In fs LA, the electron impact ionization and strong electric field ionization (photoionization) are the major processes for free electron generation, while the Coulomb explosion (gentle ablation) and thermal vaporization (strong ablation) are the two major competing mechanisms resulting in material removal and ablation.[32] However, the relaxation of the material excited by an intense femtosecond laser pulse has been quite complex which is also characterized by phase explosion and fragmentation processes.[33–37] According to Perez and Lewis,[35] spallation, homogeneous nucleation, fragmentation, and vaporization can occur simultaneously in the different regions of the target after fs laser excitation. Thermal vaporization produces mostly atomic plume, as temperatures of the emitted species are near the vaporization point of the bulk. The spectral features noticed for the slower component followed a broadband, incandescent-like emission and it is given by nanoparticles. Hence, two component emission structure noticed for fs LA are emission from excited atoms which constitute faster component and nanoparticle plume which is always attached to the target with a longer persistence. Noel *et al.*[6] reported that the ablation efficiency of fs laser is related strongly to generation of nanoparticles. At early times, the atomization is larger due to high temperature near the target surface and ablation efficiency is lower as the heat diffusion towards the bulk is larger. Because of heat diffusion to the bulk and at lower temperatures, the deeper layers are not fully atomized, instead they are ejected in the form of a mixture of gas and liquid (nanoparticles).

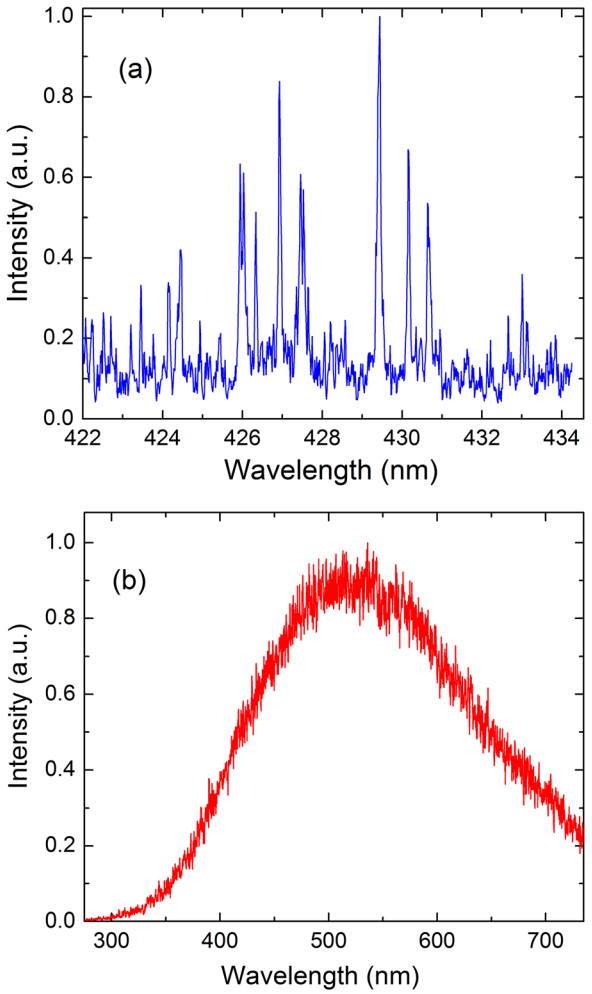

FIG. 3. Emission spectral features from (a) fast and (b) slow components are given. Both the spectra were recorded at 1 mm from the target and at times 200 ns and 2 μs delay times, respectively, for fast and slow components with gate widths 10 ns and 1 μs.

The nanoparticles emitted during fs LA of W showed broadband emission. Figure 4 shows the emission features of W nanoparticle plume recoded at different time delays with respect to the laser pulse and recorded at 2 mm from the target surface. The continuum emission spectra given in Figure 4 are not corrected for spectral response curve of the detection system. The broadband spectral features given in Figure 4 can be used for estimating particle temperature by assuming Plank's radiation spectrum. According to Ref. 19, for smaller particles with $2\pi a/\lambda < 3$ (where a is the particle radius and λ is the emission wavelength), the nanoparticle emissivity $\varepsilon(a,\lambda)$ will be proportional to a^3/λ and with $hc/\lambda \gg K_B T$, the recorded emission intensity $I(a,\lambda)$ is approximately following:

$$I(a,\lambda) \propto \lambda^{-5} \exp\left(-\frac{hc}{\lambda K_B T}\right), \quad (1)$$

where T is particle temperature, h and K_B are Planck and Boltzmann constants, and c is velocity of light. The temperature of the nanoparticles can be estimated from the slope of semi log plots of $I\lambda^5$ against $1/\lambda$. Typical semi log plot obtained from spectral response corrected broadband

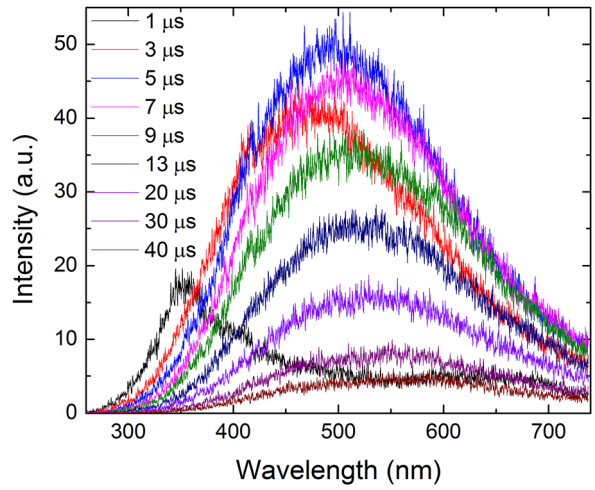

FIG. 4. Emission spectra of W plume recorded at different times after its generation. A 10% gate width of delay time was used for spectral measurement and all spectra were obtained at a distance 2 mm from the target surface. The given spectra are not calibrated for spectral response curve for spectrograph optics and detector response.

spectrum recorded at 2 mm from the target at a delay time of 5 μs is given in Figure 5(a) which shows correlation coefficient $R^2 > 0.99$. The estimated particle temperatures at different times after the evolution of W plume is given in Figure 5(b). Similar reduction in temperature with space and time was also observed for Si nanoparticles during ultrafast laser ablation of Si.[19] The particle temperatures estimated at increasing time delays with respect to laser pulse showed a t^{-1} dependence indicating the rapid cooling of the nanoparticle during vacuum expansion. It has to be pointed out that the nanoparticle temperature decay given in Fig. 5(b) was obtained from the blackbody radiation curves which were collected from a specific observation point in the plume and hence do not represent the temperature decay of an ensemble of particle. The recorded temperature variation can be related to different groups of nanoparticles come from the relaxation of different material parts located at different depths into the pristine target starting at different temperatures.[38] The melting and evaporation temperatures of W are 3422 °C and 5555 °C, respectively, and the recorded particle temperature at earliest times (<2 μs) is found to be higher than that of the melting temperature. It implies that the measured spectral features at early times are not solely due to W nanoparticles alone. Plasma produced from high-Z materials like W emits broad continuum emission for a prolonged time. The spectral features observed at 1 μs evidently shifted to shorter wavelength ~350 nm (Figure 4) with an appearance of weak nanoparticle thermal peak at ~550 nm. However, typically, the continuum emission from fs laser ablated plasmas are significantly lower compared to ns laser ablated plasma.[29] Hence, the appearance of broad peak at shorter wavelength can be contributed by cluster and molecular emission.[39] It is also possible that the higher particle temperature observed at early times could also be due to hot droplet splashing from molten material.

The ICCD images showed intense emission from nanoparticles at delayed times. We have also examined the optical time of flight (OTOF) of nanoparticle emission. For this

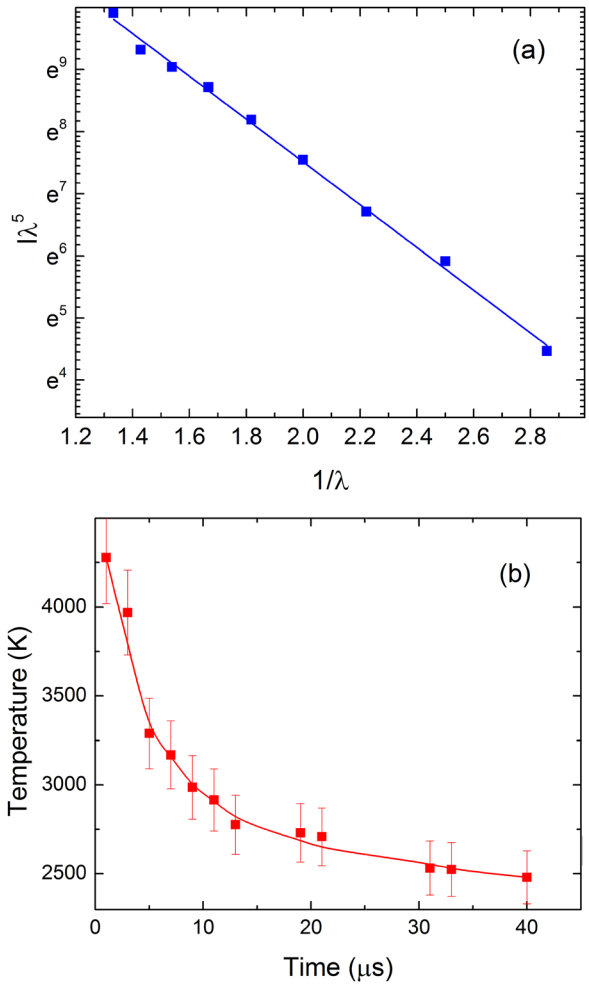

FIG. 5. (a) Typical example of semilogarithmic plot of $I\lambda^5$ vs λ^{-1} for particle temperature estimate is given in (a). The data are obtained from spectral response corrected broadband emission features recorded at 2 mm from the target and at a delay time of 5 μs. In (b), the estimated particle temperatures are given for different times.

purpose, we collected the temporal profile of the incandescent emission at 327 nm and it is given in Figure 6. The measurements were made at 2 mm away from the target surface. The temporal profile shows sharp W ion peak emitting

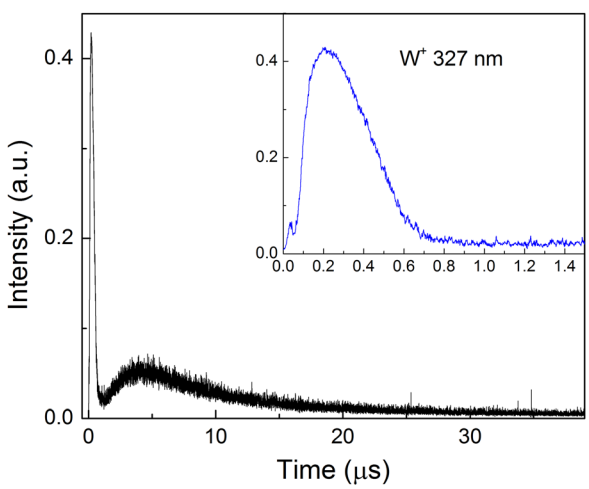

FIG. 6. OTOF profiles recorded at 327 nm wavelength. The W^+ emission is seen at the earliest time (inset) followed by a broad nanoparticle emission.

at 327 nm followed by a delayed peak which persists for a very long time. At 2 mm, the delay time for peak emission of W^+ and nanoparticles are 175 ns and 4.5 μs which correspond to a velocity of 11.4×10^5 cm/s and 4×10^4 cm/s, respectively. The measured velocity of plasma plume species and nanoparticles using OTOF agrees reasonably well with the estimated velocity from the ICCD images. We also evaluated the size distribution of W nanoparticles using a witness plate positioned 3 cm away from the target surface and performed post analysis using an AFM and results showed that the size distribution peaked ~30 nm.

The spectral features of W plume showed intense nanoparticle emission at later times. Comparing the emission features of W nanoparticles with Si particles reported in Ref. 19, the nanoparticle plume emission as well as broadband spectral emission from W seems to be very intense. However, a direct comparison between the W and Si nanoparticle plume intensity is difficult considering nearly an order of magnitude differences in the laser fluence used in Ref. 19 and present study. We, therefore, compared the features of Si nanoparticles under similar experimental conditions used for W ultrafast ablation. The ICCD images of Si nanoparticles and broadband emission features recorded during ultrafast laser ablation of Si are given in Figure 7. ICCD images were obtained using a gate width of 10% of gate delay. The broadband spectral features of Si nanoparticle plume and temperature estimate of the particles at different moments after plasma generation are given in Figure 8. Compared to W nanoparticle plume emission, the emission from Si nanoparticles is found to be significantly less intense and persistence is limited to 10's of microseconds rather 100's of microseconds noticed in the case of W nanoparticles. In the case of Si target, the estimated particle temperature at 1 μs is greater than evaporation temperature. The estimated particle temperature at any instant after the fs laser ablation is found to be higher for W compared to Si. The particle temperature with time followed $t^{-0.9}$ dependence for Si nanoparticle plumes. The temperature estimate also showed W particles are consistently higher at any time moment compared to Si particles. The melting and evaporation temperatures for Si and Ware (1414 °C, 2900 °C) and (3422 °C, 5555 °C), respectively. Hence considering nanoparticle emission is coming directly from the bulk, the temperatures of ablation region will be considerably higher for W compared to Si. So higher melting temperatures of W may be the reason of observed higher particle temperatures compared to Si (Figs. 5 and 7).

The significantly enhanced broadband emission from W compared to Si target could be related to nanoparticle generation and yield. The ablation crater depth and volume is the byproduct of both plasma species and nanoparticle ejection. Hence, the ablation efficiency of a target material is related to both atom and nanoparticle emission. Regardless of the target material, at early times the atomization is larger due to high temperature near the target surface and ablation efficiency from atomic emission is lower as the heat diffusion towards the bulk is larger. Because of heat diffusion to the bulk and the resulting lower temperatures, the deeper layers are not fully atomized, instead they are ejected in the form of

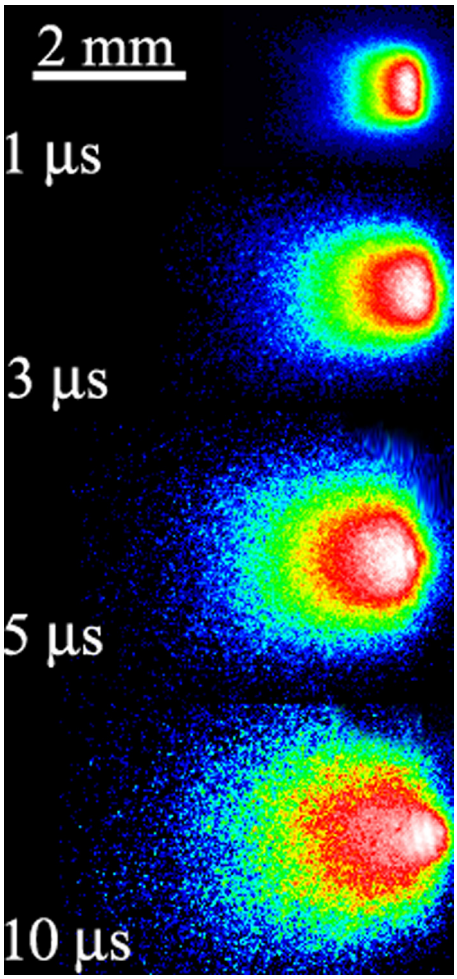

FIG. 7. Images of Si nanoparticle plume obtained using ICCD at various times after the onset of plasma plume generation. The plume was generated using 40 fs, 800 nm ultrafast laser in vacuum. The ICCD gating was set at 5% of gate width and each image was normalized to its maximum intensity for better view.

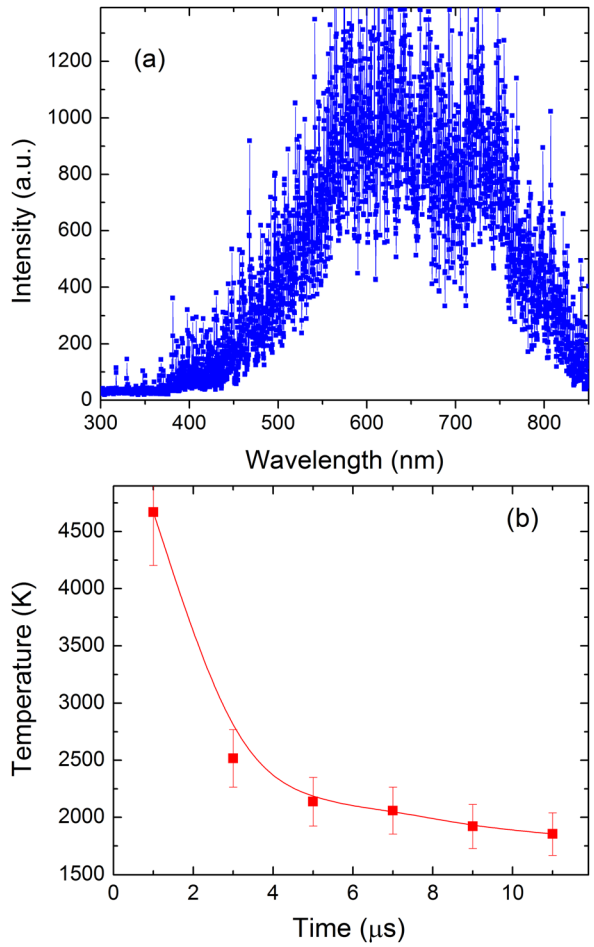

FIG. 8. (a) Typical broadband spectral emission from Si nanoparticle recorded 5 μs after the onset of plasma generation is shown and in (b) the particle temperature estimate at 1 mm from the spectral response corrected broadband emission is provided.

nanoparticles.[6] Compared to ns or ps pulse duration, the pulses in the fs regime typically provide higher ablation efficiency because of lack of laser-plasma interaction and energy loss. This is because, in fs LA, the laser pulse terminates before the plasma generation.[40] Hence, the fs absorbed energy will heat the target to solid density plasma state with high temperature and density above the critical point.[19] Since similar laser ablation conditions are used for W and Si, the observation of brighter nanoparticle plume for W compared to Si could be related to material properties. So it has to be highlighted that under ultrafast laser irradiation conditions, the ablation processes are strongly dependent on the material nature. The absorption processes as well as ablation physics are different for metal, semiconductor, and dielectric materials.[21] In metals, free electrons in the conduction band absorb energy through inverse Bremsstrahlung process. For semiconductor, valence band electrons absorb photons and move to conduction band through multi-photon absorption. If they do not have enough energy to reach the next energy level in the conduction band, the electrons generally decay to their initial state and reemit the photon. The reported ablation threshold for Si and metal targets using ultrafast lasers are in the range $\sim$0.2–0.5 J/cm^2.[21,41] Hence, considering both the experiments are performed at significantly higher energy fluence (8 J/cm^2) than the ablation threshold, the laser energy coupling to the target will be similar and hence the ablation threshold differences may not explain the differences noticed in nanoparticle emission features between W and Si. Ultrafast laser energy transport to the target (electrons) is extremely fast and happens during the laser pulse. The electrons will eventually transfer energy to lattice/ions and time scales of these events are represented by characteristic relaxation times. Typically the electron-ion relaxation time (τ_{ei}) depends on the heaviness of ions (for example, W$\tau_{ei} \gg$ Si τ_{ei}).

We compared the craters generated by ultrafast laser ablation of W and Si under similar conditions and results showed deeper craters for Si compared to W (images not given). Previous studies highlighted that the ablation efficiency is higher for metals with lower melting point and hardness.[40] Noel *et al.*[6] compared the intensity of atomization (I_{atoms}) and nanoparticle (I_{nps}) ejection from Cu and Au targets and found that atomization is higher for Cu while nanoparticle ejection is higher for Au and attributed this to high electron-lattice coupling coefficient (G) values of Cu compared to Au ($G_{cu} = 1 \times 10^{17}$ Wm^{-3}K^{-1}, $G_{Au} = 2.1 \times 10^{16}$ Wm^{-3}K^{-1}). However, a close comparison between

the material properties of W and Si do not yield the reasoning for higher nanoparticle plume emission from W, we conducted similar studies in other low-Z and high-Z metals which included Al, Cu, Mo, and Ta. Comparing the nanoparticle broadband emission features studied among the target materials, W and Ta provided most intense emission features followed by Mo, while Cu and Al showed significantly lower nanoparticle emission intensity which was similar to Si target. This trend is approximately similar to melting and evaporation temperatures of various materials studied; higher nanoparticle plume intensity noticed for targets with higher melting or evaporation temperatures. However, further studies are necessary to explain the role of each physical and thermal properties on nanoparticle yield. Apart from melting and evaporation temperatures, the role of other parameters, e.g., target density, electron-lattice coupling coefficient, electron-ion relaxation times, etc., may affect the nanoparticle ejection and hence further detailed research studies are essential to elucidate the role of each physical and thermal parameters on nanoparticle yield from fs laser ablation plumes.

IV. CONCLUSIONS

We investigated the expansion features of ultrafast laser generated nanoparticle plumes in vacuum. The ICCD fast-gated images showed two distinct features of component expansion generated by W plasma and nanoparticle plumes, separated in time. The ICCD images also showed that the emission from atomic plume persisted $\sim$400 ns while the nanoparticle plumes persisted for a prolonged time which was about $\sim$100 μs. The expansion velocity estimate showed that the nanoparticle plume moved at a significantly lower velocity compared to plasma plume and the expansion velocities were differed by $\sim$25 times. The temperature of the nanoparticles generated showed that a decreasing trend with increasing time and space. A comparison with Si nanoparticle plume showed that under similar experimental conditions, ultrafast laser ablation of high-Z materials like W provided significant higher nanoparticle yield. The differences in nanoparticle yield could be related to evaporation and melting temperature, however, further research efforts are necessary to explain the role of other material parameters on nanoparticle yield.

ACKNOWLEDGMENTS

This work was partially supported by the U.S. National Science Foundation (NSF) Partnerships for International Research and Education (PIRE) program.

[1]H. M. Joshi, J. Nanopart. Res. **15**, 1235 (2013).
[2]B. Luo, S. Liu, and L. Zhi, Small **8**, 630 (2012).
[3]T. X. T. Sayle, P. E. Ngoepe, and D. C. Sayle, ACS Nano **3**, 3308 (2009).
[4]J. Perez-Juste, I. Pastoriza-Santos, L. M. Liz-Marzan, and P. Mulvaney, Coord. Chem. Rev. **249**, 1870 (2005).
[5]B. Wu, Y. Kuang, X. Zhang, and J. Chen, Nanotoday **6**, 75 (2011).
[6]S. Noel, J. Hermann, and T. Itina, Appl. Surf. Sci. **253**, 6310 (2007).
[7]S. Amoruso, R. Bruzzese, M. Vitiello, N. N. Nedialkov, and P. A. Atanasov, J. Appl. Phys. **98**, 044907 (2005).
[8]C. L. Sajti, R. Sattari, B. N. Chichkov, and S. Barcikowski, J. Phys. Chem. C **114**, 2421 (2010).
[9]J. Perriere, C. Boulmer-Leborgne, R. Benzerga, and S. Tricot, J. Phys. D **40**, 7069 (2007).
[10]D. Scuderi, O. Albert, D. Moreau, P. P. Pronko, and J. Etchepare, Appl. Phys. Lett. **86**, 071502 (2005).
[11]B. Tan and K. Venkatakrishnan, Opt. Express **17**, 1064 (2009).
[12]R. Teghil, L. D'Alessio, A. De Bonis, A. Galasso, P. Villani, and A. Santagata, Thin Solid Films **515**, 1411 (2006).
[13]U. Chakravarty, P. A. Naik, C. Mukherjee, S. R. Kumbhare, and P. D. Gupta, J. Appl. Phys. **108**, 053107 (2010).
[14]B. Kumar and R. K. Thareja, Phys. Status Solidi C **7**, 1409 (2010).
[15]M. Sivayoganathan, B. Tan, and K. Venkatakrishnan, Opt. Mater. Express **2**, 987 (2012).
[16]M. K. Moodley and N. J. Coville, Chem. Phys. Lett. **498**, 140 (2010).
[17]B. Liu, Z. D. Hu, Y. Che, Y. B. Chen, and X. Q. Pan, Appl. Phys. Lett. **90**, 044103 (2007).
[18]K. F. Al-Shboul, S. S. Harilal, and A. Hassanein, Appl. Phys. Lett. **100**, 221106 (2012).
[19]S. Amoruso, G. Ausanio, R. Bruzzese, M. Vitiello, and X. Wang, Phys. Rev. B **71**, 033406 (2005).
[20]J. Hermann, S. Noel, T. E. Itina, E. Axente, and M. E. Povarnitsyn, Laser Phys. **18**, 374 (2008).
[21]E. G. Gamaly, *Femtosecond Laser-Matter Interactions* (Pan Stanford Publishing, Singapore, 2011).
[22]K. Oguri, Y. Okano, T. Nishikawa, and H. Nakano, Phys. Rev. B **79**, 144106 (2009).
[23]T. E. Glover, G. D. Ackerman, R. W. Lee, H. A. Padmore, and D. A. Young, Chem. Phys. **299**, 171 (2004).
[24]S. Amoruso, R. Bruzzese, C. Pagano, and X. Wang, Appl. Phys. A **89**, 1017 (2007).
[25]K. F. Al-Shboul, S. S. Harilal, and A. Hassanein, J. Appl. Phys. **113**, 163305 (2013).
[26]P. K. Diwakar, S. S. Harilal, N. L. LaHaye, A. Hassanein, and P. Kulkarni, J. Anal. At. Spectrom. **28**, 1420 (2013).
[27]B. Lukyanchuk, N. Bityurin, S. Anisimov, and D. Bauerle, Appl. Phys. A **57**, 449 (1993).
[28]R. K. Singh and J. Narayan, Phys. Rev. B **41**, 8843 (1990).
[29]B. Verhoff, S. S. Harilal, J. R. Freeman, P. K. Diwakar, and A. Hassanein, J. Appl. Phys. **112**, 093303 (2012).
[30]S. S. Harilal, J. Appl. Phys. **102**, 123306 (2007).
[31]F. Nazar, S. S. Harilal, H. Ding, and A. Hassanein, Appl. Phys. Lett. **103**, 191112 (2013).
[32]R. Stoian, D. Ashkenasi, A. Rosenfeld, and E. E. B. Campbell, Phys. Rev. B **62**, 13167 (2000).
[33]S. Amoruso, R. Bruzzese, X. Wang, N. N. Nedialkov, and P. A. Atanasov, J. Phys. D **40**, 331 (2007).
[34]J. P. Colombier, P. Combis, R. Stoian, and E. Audouard, Phys. Rev. B **75**, 104105 (2007).
[35]D. Perez and L. J. Lewis, Phys. Rev. B **67**, 184102 (2003).
[36]M. E. Povarnitsyn, T. E. Itina, M. Sentis, K. V. Khishchenko, and P. R. Levashov, Phys. Rev. B **75**, 235414 (2007).
[37]T. E. Itina, K. Gouriet, L. V. Zhigilei, S. Noel, J. Hermann, and M. Sentis, Appl. Surf. Sci. **253**, 7656 (2007).
[38]S. Amoruso, R. Bruzzese, N. Spinelli, R. Velotta, M. Vitiello, and X. Wang, Europhys. Lett. **67**, 404 (2004).
[39]S. Amoruso, G. Ausanio, M. Vitiello, and X. Wang, Appl. Phys. A **81**, 981 (2005).
[40]A. Semerok, C. Chaleard, V. Detalle, J. L. Lacour, P. Mauchien, P. Meynadier, C. Nouvellon, B. Salle, P. Palianov, M. Perdrix, and G. Petite, Appl. Surf. Sci. **138**, 311 (1999).
[41]J. Bonse, S. Baudach, J. Kruger, W. Kautek, and M. Lenzner, Appl. Phys. A **74**, 19 (2002).